JOURNAL OF SPACECRAFT AND ROCKETS
Vol. 47, No. 4, July–August 2010

Computational Procedure for the Life Assessment of Solid Rocket Motors

Şebnem Özüpek*
Boğaziçi University, 34342 Istanbul, Turkey

DOI: 10.2514/1.46801

A computational procedure for service-life estimation of a solid propellant rocket motor grain is developed. The propellant response is mathematically represented using a nonlinear damaging viscoelastic model. A finite element analysis is then performed to identify potential failure modes of the grain and to determine the critical values of stress–strain associated with the potential failure modes. Both the current and aged propellant samples are calibrated and the motor is analyzed for the models representing the different ages of the motor. Based on the available strain capability and bond-line strength data, the grain service life is estimated to end by bond failure during cold firing.

Nomenclature

a_T	=	shift function
C_i, T_r	=	Williams–Landel–Ferry coefficients and reference temperature [Eq. (14)]
c	=	void content
E	=	Young's modulus, kg/mm^2
f	=	cyclic loading function
$G(t)$	=	relaxation function
g	=	damage function
$\bar{I}_\gamma$	=	distortional deformation
$\bar{I}_1$, $\bar{I}_2$	=	deviatoric invariants of Cauchy strain tensor
J	=	volume change ratio
K	=	bulk modulus, kg/mm^2
K_0	=	initial bulk modulus, kg/mm^2
$\bar{\mathbf{S}}$, σ	=	viscoelastic stresses
$\bar{\mathbf{S}}_e$, $\hat{\sigma}_e$	=	elastic stresses
s_i	=	internal state variables
α	=	thermal expansion coefficient, 1/°C
β_i, ω_i, n	=	model parameters
ν	=	Poisson's ratio
ϕ	=	strain energy function
$\bar{\phi}$	=	distortional part of the strain energy function
$\hat{\phi}$	=	dilatational part of the strain energy function

Introduction

SERVICE-LIFE estimation of a solid propellant rocket motor consists of identifying the most critical failure modes and determining when the properties of motor components degrade to a point where failure is predicted. One possible method for determining failure modes is experimentally based and comprises thermally overtesting full-scale or subscale motors. This approach is expensive and impractical, due to the limited availability of in-service motors, the difference of failure modes between subscale and full-scale motors, and varying loading conditions to which the rocket may be subjected during its lifetime. An alternative approach is based on the use of computational techniques such as the finite element method. This approach allows the investigation of various failure modes under several loading conditions without the expenditure of motors. Of course the accuracy of the prediction depends on the accuracy of input data, failure data, and mathematical models.

The life-assessment procedure described in this study is computationally based and comprises essentially two tasks. The first, and by far the more demanding of these, is the finite element analysis (FEA) for the determination of the stresses, strains, and damage induced in the grain by the various thermal and pressure loadings. The second task consists of evaluating the results of the FEA as they affect the prediction of the probable service life of the motor.

The most challenging aspect of the FEA of the motor is the representation of the highly nonlinear response of the solid propellant, which is composed of an elastomeric binder filled with a high percentage of much stiffer particles. The large range of deformations, viscoelastic effects, debonding of particles from the binder, transition from incompressible to compressible behavior, coupling between dilatational and distortional behavior, and nonlinearities during cyclic loading are typical features of propellant mechanical response. Representation of these phenomena has been the subject of a number of previous investigations. Although several constitutive models have been proposed, the following review is concerned with those that are readily applicable to three-dimensional behavior and hence can be incorporated in a numerical stress analysis. One of the first three-dimensional finite viscoelastic models incorporating damage is due to Simo [1]. The uncoupling of volumetric and deviatoric responses and the associated computational framework developed in this work have been used by many researchers. Özüpek and Becker [2] introduced a strain softening function into Simo's model to account for the damage effect in stress response. A later study by the same authors [3] proposed a dilatation model, which represents the formation and growth of voids and the effects of distortion and superimposed pressure on the volume change of the propellant. Jung and Youn [4] modeled the softening due to damage by changing the modulus based on filler volume fraction. A computational damage evolution model proposed by Matouš and Geubelle [5] incorporates a multiscale approach to predict debonding of particles from the binder. Areias and Matouš [6] focused on the response of the elastomeric binder and proposed a model that captures the viscous flow due to stress concentrations in the vicinity of the particles. The particle-matrix debonding is not incorporated in the model. This effect (also called dewetting), which is characteristic of propellant behavior, is the emphasis of work by Xu et al. [7] in which physically justified model parameters were used. Other works concerned with the constitutive modeling of solid propellants are reviewed in the literature stated above.

Contrary to the amount of work concerned with the constitutive modeling of solid propellants, very few studies are found in the open literature concerning the use of these equations in the stress analysis of the propellant grain and their implications for a motor's structural

Received 20 August 2009; revision received 26 April 2010; accepted for publication 20 May 2010.

*Department of Mechanical Engineering; ozupek@boun.edu.tr.

failure. Chyuan [8] studied the effect of thermal loading on propellant failure using a maximum-principal-stress failure criterion. The propellant is modeled as linear viscoelastic and the factor of safety to be used in design is calculated. In a later work Chyuan [9] developed a nonlinear simulation of the grain subjected to thermal loading by considering bulk modulus variation with compressive stresses. The simulation shows that the effect of nonlinear bulk modulus becomes more important at temperatures higher than the stress-free temperature of the grain.

Characterization of propellant aging is an important aspect of service-life assessment, since both the material response and capabilities may change with age. Christiansen et al. [10] used a time-aging time superposition similar to time–temperature superposition to predict real-time aging based on accelerated aging test data and the Arrhenius equation. Kivity et al. [11] established the temperature range of accelerated aging tests for which the Arrhenius equation holds. Methods correlating real-time and accelerated aging are still under investigation [12], and an aging constitutive model is not yet available in the literature.

When a realistic constitutive model of the propellant is available, stress–strain response and capabilities are accurately evaluated and represented as a function of age, the service life of the rocket can be confidently predicted. Hardly any study is reported in the literature describing a complete methodology for service-life estimation. Ho [13] studied the bond-line failure and propellant cracking by measuring the dynamic mechanical properties of samples from a rocket motor. The method allows evaluation of motor components to environmental loadings seen in the motor during its service life. The methodology proposed by Collingwood et al. [14] is based on a nonlinear viscoelastic analysis, incorporates aging trends and uses a probabilistic approach to the service-life estimation. The comparative evaluation of different nonlinear viscoelastic approaches shows the necessity to accurately account for the volumetric behavior of the propellant.

The service-life estimation methodology proposed in this paper first aims to represent major features of solid propellant behavior. The material model selected for this purpose is applicable over any range of deformations and incorporates viscoelasticity, damage, and dilatation model. Second, the proposed procedure aims to account for mechanical response changes due to aging by regularly monitoring the propellant behavior and reflecting these changes in the material model. In the following, the constitutive model and its calibration for new and aged propellants are described. The rocket motor is analyzed for loading conditions that are critical to determine the long-term behavior of the propellant grain. The temperature and pressure conditions for these loadings and the finite element analysis results are presented. The final objective of the proposed methodology is the quantitative prediction of the grain lifetime. This is done based on an approach that uses the finite element analysis results and the experimental capability data.

Finite Element Modeling

The solid rocket motor considered in this work is a circular-port case-bonded configuration with a stress-relieving slot in the head end and a boot in the aft end. The motor case is fiber-reinforced plastic. The case interior is covered with an insulator that is an ethylene propylene diene M-class (EPDM) rubber. The propellant grain is bonded to the insulation by a liner that has a composition similar to that of the propellant. The grain and case are axisymmetric, as are all of the finite element models and analyses done in this work.

The goals of the finite element analysis are to identify potential failure modes of the grain and to determine the critical values of stress–strain associated with the potential failure modes for the models representing the different ages of the motor.

Although failure may occur under any of the variety of storage and operational loads to which the solid rocket motor is subjected, thermal loads resulting from the exposure to diurnally and seasonally varying temperature conditions usually represent the most demanding long-term load environment. It is well known that propellant under this cyclic type of loading conditions fails under loads that are substantially lower than those determined from standard laboratory tests. The latter typically do not account for the long-term degradation effects on the failure properties, due to the laboratory test-time limitation and the use of specimens prepared during the production of the propellant. To investigate the stress–strain state under thermal loads, two thermal-cycling profiles were considered, as described later in the paper. Since the motor case is a composite, and hence has a low stiffness, pressure loads may also play a significant role in failure. Therefore, the stress–strain state resulting from ignition pressurization was also investigated.

The entire analysis procedure was performed using the commercially available finite element software TEXPAC [15]. The code is designed specifically for the structural analysis of elastomeric structures, and the propellant constitutive model has been implemented in this code.

Finite Element Mesh

The geometry of the motor was available in the form of CAD files. These files were imported into the finite element software package and were used there to create the finite element mesh shown in Fig. 1. The mesh consisted of quadratic isoparametric quadrilateral elements. The propellant, liner, and insulation were modeled using nine-node reformulated elements. The aluminum parts and the motor case were modeled using eight-node quadrilaterals with reduced integration.

Material Models

Material characterization consisted of the determination of material properties for the motor case, boss, solid propellant, insulation and liner. The fiber-reinforced case and the aluminum boss were modeled as isotropic linear elastic materials with the following values:

Case:

$$E = 4615\ \text{kg/mm}^2, \qquad \nu = 0.33, \qquad \alpha = 2.304\text{e}-6\ 1/^\circ\text{C}$$

Aluminum:

$$E = 7031\ \text{kg/mm}^2, \qquad \nu = 0.33, \qquad \alpha = 22.5\text{e}-6\ 1/^\circ\text{C}$$

The properties of the fiber-reinforced case are actually anisotropic and vary from point to point. However, only isotropic and homogeneous properties given above were available. The consequence of this assumption is discussed at the end of the paper.

The propellant, liner, and insulation are elastomeric components. The propellant properties described below were also used for the liner. The insulation made of EPDM was represented as a hyperelastic NeoHooken material with strain energy function $U = C(\bar{I}_1 - 3) + K/2(J-1)^2$. The model data consisted of $C = 0.05\ \text{kg/mm}^2$, $K = 200\ \text{kg/mm}^2$, and $\alpha = 1.8\text{e}-4\ 1/^\circ\text{C}$.

Constitutive Model of Solid Propellant

The constitutive model for the propellant is a nonlinear viscoelastic representation based on a phenomenological approach. It is applicable to large deformations and rotations. There is a significant coupling between volumetric and deviatoric responses. The representation employs a dilatation model that accounts for the formation and growth of voids at or near the binder–particle interface. The effects of distortion and superimposed pressure on volume change are incorporated through the dilatation model. Softening due to damage and nonlinearities during cyclic loading are also accounted for in the constitutive representation.

The motivations in formulating the model, its development and its computational implementation in the finite element code TEXPAC are described in detail in Canga et al. [16]. In the following, a summary of the formulation and the calibration of the model parameters are given.

The elastic response of the propellant material is derived from a strain energy function defined as

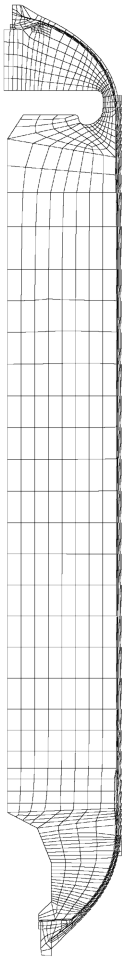

Fig. 1 Finite element mesh of the motor.

$$\phi = g(s_1) f(s_2, s_3) \bar{\phi}(\bar{I}_1) + \hat{\phi}(J, c) \tag{1}$$

where the void content c results from dewetting at the particle–binder interface. The elastic stresses $\bar{\mathbf{S}}_e$ and $\hat{\sigma}_e$ are derived as

$$\bar{\mathbf{S}}_e = g f \partial \bar{\phi} / \partial \mathbf{E}, \qquad \hat{\sigma}_e = \partial \hat{\phi} / \partial J \tag{2}$$

The distortional part of the strain energy function of the undamaged material consists of a Rivlin polynomial plus an exponential term that represents the toe region in the test data of some propellants

$$\bar{\phi} = \sum_{i=1}^{4} \beta_i (\bar{I}_1 - 3)^i + \frac{\beta_5}{\beta_6} (1 + e^{-\beta_6 (\bar{I}_1 - 3)}) \tag{3}$$

The damage of the propellant is assumed to be irreversible and is measured by s_1, which is a nondecreasing function of the void content c:

$$s_1 = \max_{0 \le \tau \le t} c(\tau) \tag{4}$$

The damage function g, is a nonincreasing function of damage parameter s_1. The void content c varies according to

$$\dot{c} = \dot{\gamma} e^{\hat{\sigma}_e / \omega_2}, \qquad \gamma = \omega_1 \bar{I}_\gamma^n, \qquad c(0) = 0 \tag{5}$$

where

$$\bar{I}_\gamma = \tfrac{1}{6}(2\bar{I}_1^2 - 6\bar{I}_2) \tag{6}$$

The dilatational part of the strain energy function is of the form

$$\hat{\phi} = \tfrac{1}{2} K(c) (J - 1)^2 \tag{7}$$

where K varies with the void content c, according to

$$\frac{\mathrm{d}K(c)}{\mathrm{d}c} = -\frac{K}{(1 - c)} (1 + \omega_3 K) \quad \text{with} \quad K(0) = K_0 \tag{8}$$

The cyclic loading function $f\ (s_2, s_3)$ has three distinct branches:

$$f = \begin{cases} 1 & \text{loading} \\ f_u & \text{unloading} \\ f_u + s_3 (f_r - f_u) & \text{reloading or unloading from reloading} \end{cases} \tag{9}$$

The internal state variable s_2 depends on the amount of distortional deformation $\bar{I}_\gamma$:

$$s_2 = \bar{I}_\gamma / \bar{I}_\gamma^l \quad \text{with} \quad \bar{I}_\gamma^l = \max_{0 \le \tau \le t} \bar{I}_\gamma \text{ during loading} \tag{10}$$

The internal state variable s_3 is introduced to smooth out the transition between the different branches and is defined as

$$s_3 = \begin{cases} (\bar{I}_\gamma - \bar{I}_\gamma^u)/(\bar{I}_\gamma^l - \bar{I}_\gamma^u) & \bar{I}_\gamma^u < \bar{I}_\gamma < \bar{I}_\gamma^l \\ 1 & \bar{I}_\gamma > \bar{I}_\gamma^l \end{cases} \tag{11}$$

where $\bar{I}_\gamma^u = \min_{0 \le \tau \le t} \bar{I}_\gamma$ during unloading.

The viscoelastic stresses $\bar{\mathbf{S}}$ and σ are obtained by using hereditary integrals on the elastic stresses $\bar{\mathbf{S}}_e$ and σ_e:

$$(\bar{\mathbf{S}}, \sigma) = \int_0^t G(t - \tau) \frac{\partial (\bar{\mathbf{S}}, \sigma)_e}{\partial \tau} \, \mathrm{d}\tau \tag{12}$$

The relaxation function $G(t)$ is represented as a Prony series:

$$G(t) = G_\infty + \sum_{j=1}^{m} G_j e^{-t/\tau_j} \tag{13}$$

Thermorheologically simple behavior is assumed and the time–temperature equivalence implied by this assumption is incorporated through a shift function $a_T(T)$, expressed in Williams–Landel–Ferry (WLF) form [17] as

$$\log_{10} a_T = \frac{-C_1 (T - T_r)}{C_2 + (T - T_r)} \tag{14}$$

Calibration and Validation of the Propellant Constitutive Model

The constitutive model parameters were determined separately for the new and aged propellants. Both propellants have the same composition. The new propellant is at zero age, while the aged propellant is six years older. Test specimens used to determine the material response and the capability data were obtained from dissected motors.

The following calibration procedure was performed for the new propellant:

Stress relaxation tests at −60, −50, −40, −20, 0, 20, and 60°C were used to construct $G(t)$ and a_T. The tests were performed at 2% strain level using wooden tab-end bar specimens. Characteristic times τ_j were selected one decade apart and the coefficients G_j were calculated using a least-squares technique. The resulting master curve and Prony fit are shown in Fig. 2.

The coefficients of the energy function of the undamaged material, β_i, were obtained from the uniaxial tension test at 1000 psig (0.7 kg/mm^2). Since the dilatation at that pressure level is insignificant, it was assumed that no damage occurs: i.e., $g = 1$. Dilatation parameters ω_i and n and functions g and f were determined using the same computational algorithm as in the finite element code. First, an initial estimate of the damage function was obtained by using the stress and dilatation data at 0 psig. Using the initial g function an iterative procedure was performed to get dilatation parameters and a refined damage function. The cyclic loading function was set to unity. Note that parameters ω_i and n cannot be uniquely determined, in that their values depend on the initial estimates. An adjustment in the parameters was made by trial and error to get a reasonable agreement with the stress values as well. The value of K_0 was set

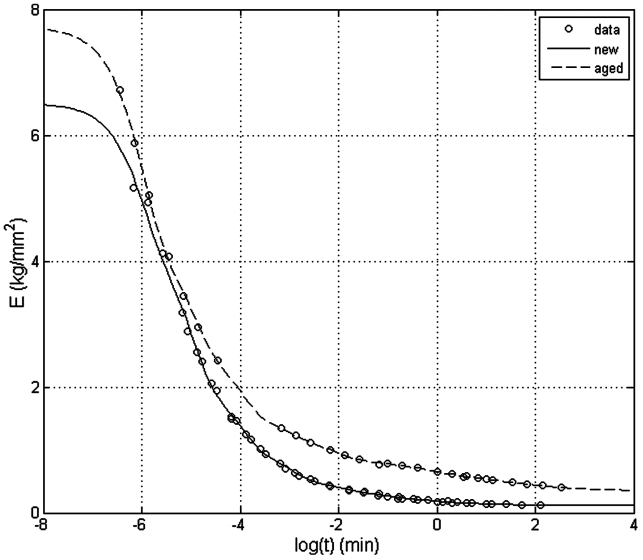

Fig. 2 Master relaxation curve for new and aged propellants.

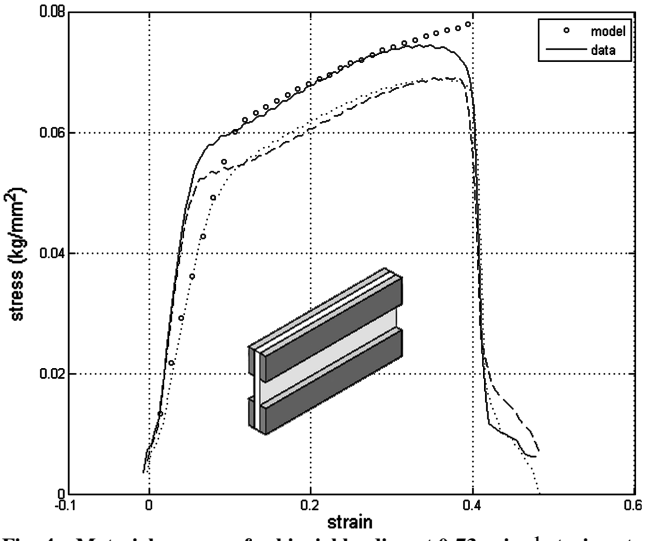

Fig. 4 Material response for biaxial loading at 0.73 min^{-1} strain rate (solid, dashed, and dotted lines represent different specimens).

equal to a previously used value of 1100 $\mathrm{kg/mm^2}$. K_0 determines the volumetric behavior before the onset of damage, that is when the propellant is incompressible. As long as K_0 is large compared to the shear modulus, its actual value does not have much influence on the overall stress–strain response. Once the propellant becomes compressible, the bulk modulus value is determined through the dilatation model described above.

Finally, using the stress data of the cycling specimen, the cyclic function f was determined in a few iterations.

The validation of the material model was carried out for uniaxial, biaxial, and analog wedge specimens. The effect of superimposed pressure on stress response is well predicted, and the dilatation response is reasonably predicted, as shown in Fig. 3. The high-pressure response becomes significant during the ignition loading, while the ambient pressure response is important in thermal loading. Both are described below in the finite element analysis of the motor. The biaxial loading and wedge-specimen predictions are in reasonable agreement with test data, as shown in Figs. 4 and 5. Biaxial and wedge tests are significant in that they show the predictive capability of the model for multi-axial stress states that are typically present in the rocket motor.

The validation of the constitutive model as described above has been carried out previously for different propellant data [3]. For each propellant, similar trends of representative capabilities were obtained.

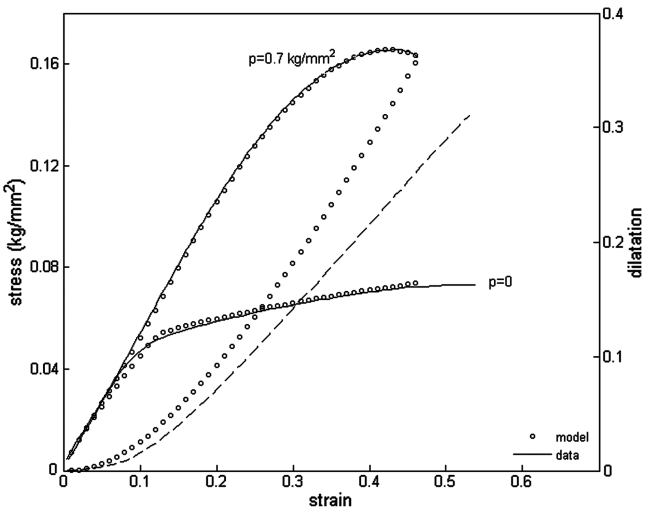

Fig. 3 Stress (solid line) and dilatation (dashed line) response for uniaxial loading with superimposed pressure at 0.73 min^{-1} strain rate.

To account for the effect of aging in the mechanical properties of the propellant, the calibration of a six-year-old propellant was carried out. The master relaxation curve was obtained from relaxation tests at −60, −20, 20, and 60°C. The Prony fit to the curve plotted in Fig. 2 shows that the relaxation modulus gets stiffer as the propellant ages, with an increase of the equilibrium modulus from 1.1714e − 01 $\mathrm{kg/mm^2}$ for the zero-age propellant to 3.6346e − 01 $\mathrm{kg/mm^2}$ for the six-year-old propellant. Uniaxial tension data at high pressure levels with no damage was not available for the aged propellant; therefore, only one coefficient was used for the energy function of the undamaged material as given in Eq. (3) and it was fitted to the initial (that is, undamaged) part of the stress–strain curve at 0 psig. The rest of the stress–strain curve and the dilatation data were used to determine the dilatation parameters and damage function. Because of the lack of data, the dilatation model could not be validated at various pressure levels.

Capability

The propellant constitutive model described above was employed in the structural analysis of the motor in order to predict the stress–strain state for the loading conditions described in the next section. To predict service life, propellant failure properties (also known as capabilities) should also be determined.

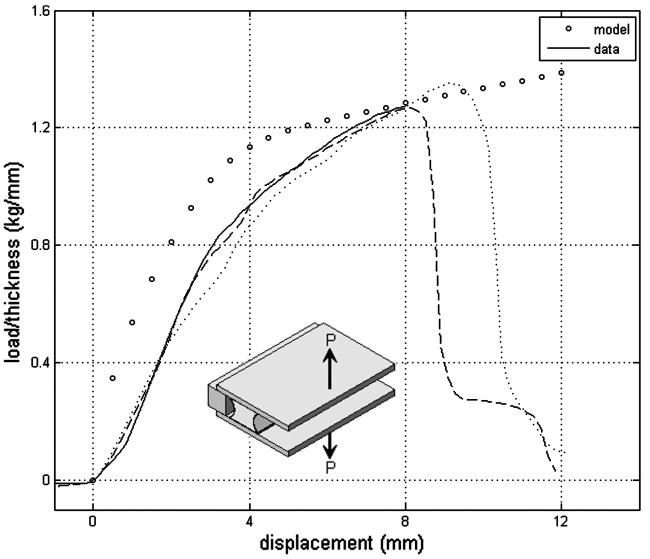

Fig. 5 Material response for analog wedge at 50 mm/min loading (solid, dashed, and dotted lines represent different specimens).

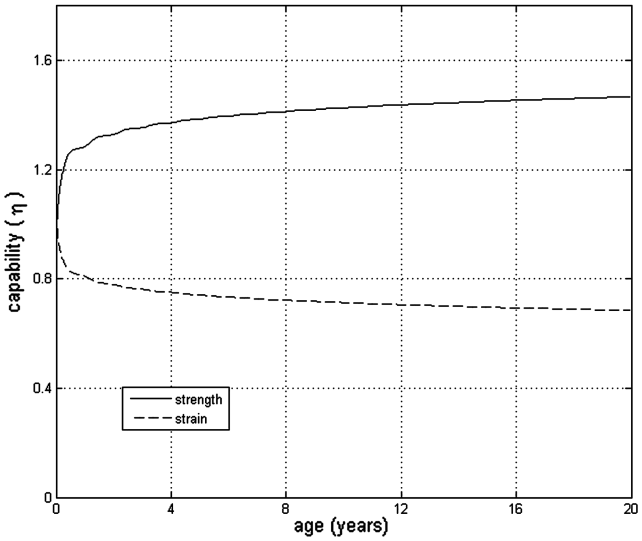

Fig. 6 Propellant capabilities [Eq. (15)] as a function of age.

Two possible failure modes were hypothesized: 1) cracking due to tensile strain at the bore and 2) liner/insulation bond failure. For strain-induced failure mode 1, strain at maximum stress, while for failure mode 2, bond-strength test results are needed. Both of these values can be extracted from uniaxial tests at various temperatures and rates and tabulated for propellants of different ages. An alternative to the above is the use of Arrhenius equations:

$$\eta(T,t) = 1 + Ae^{(-\frac{B}{T})}\,\ell_n\, t \tag{15}$$

where η represents the ratio of a propellant property that changes with age to the value of the property at zero time, t is time, T is temperature in Kelvin, and A and B are material constants. In this study Arrhenius equations were used to represent propellant strain capability and bond strength as a function of time and temperature. Material constants were determined using data from accelerated aging tests of the propellant. Aging ratios for bond strength and strain capability were determined by integrating $d\eta/dt$ for selected storage-temperature profile. The strength and strain capability changes resulting from this integration are shown in Fig. 6.

Finite Element Analysis

Three loading cases were analyzed with curing temperature of 50°C and propellant stress-free temperature of 60°C.

Thermal Cycling

Thermal cycling is assumed to represent the temperature condition in estimating the number of cycles that the motor must be able to withstand. Each five-day cycle consisted of varying the temperature between 50°C, the maximum storage temperature as well as the curing temperature, and −32°C, the lowest temperature to which the propellant may be exposed. Three cycles were analyzed, with each cycle defined as one loading step.

Three curves that report the distribution of hoop strain and of bond stress along relevant surfaces at the end of each step are shown in Figs. 7–10. The maximum hoop strain of 8.40% was observed for the new propellant at the end of the third thermal cycle on the surface of the slot region. The maximum hoop strain of 11.60% was observed for the aged propellant at the end of the second thermal cycle on the surface of the slot region. The maximum bond stress of 1.22E − 02 kg/mm^2 was observed for the new propellant at the end of the first thermal cycle at the liner–insulation interface. The maximum bond stress of 2.68E − 02 kg/mm^2 was observed for the aged propellant at the end of the first thermal cycle at the liner–insulation interface.

Thermal Storage

The solid rocket motor is subjected to diurnally and seasonally varying temperature conditions during storage. Based on a yearly temperature profile with minimum and maximum storage temperatures of −32 and 50°C, the worst-case scenario thermal loading was defined as a two-step loading. The first step was cooling down from 50°C to yearly averaged temperature. The second step was cooling down along the path corresponding to the available temperature profile from average to coldest temperature. The daily oscillations were averaged, which allowed for faster convergence of computations.

The maximum hoop strain of 6.55% was observed for the new propellant at the end of the second step on the surface of the bore region. The maximum hoop strain of 7.01% was observed for the aged propellant at the end of the second step on the surface of the bore region. The maximum bond stress of 7.82E − 03 kg/mm^2 was observed for the new propellant at the end of the second step at the liner–insulation interface. The maximum bond stress of 1.60E −

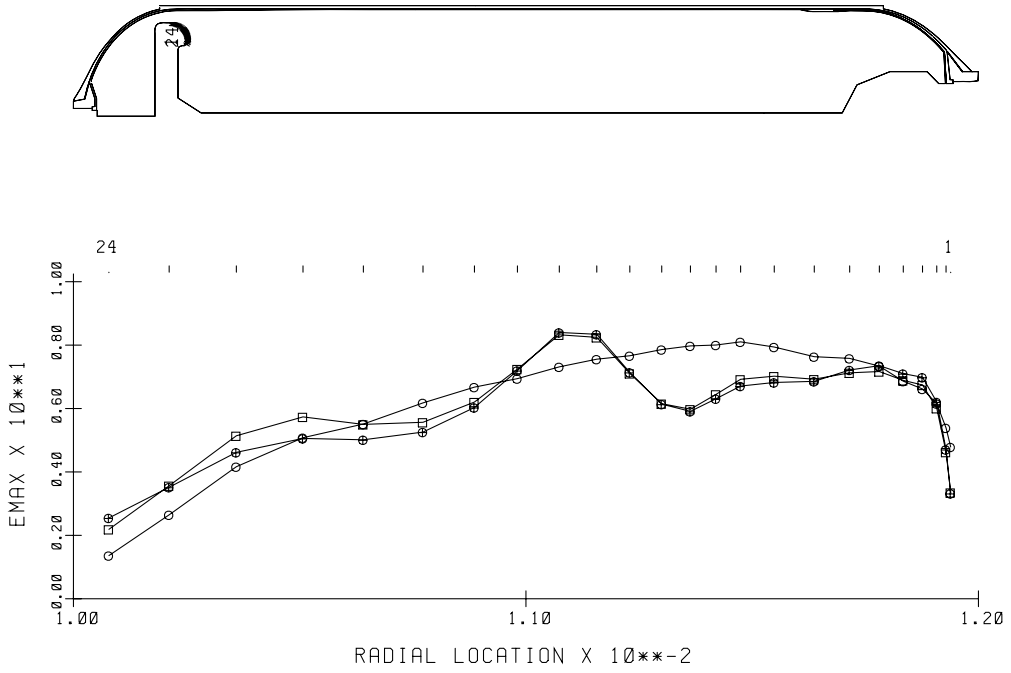

Fig. 7 Thermal-cycle hoop strains for new propellant in the slot region (first cycle ○, second cycle □, and third cycle ⊕).

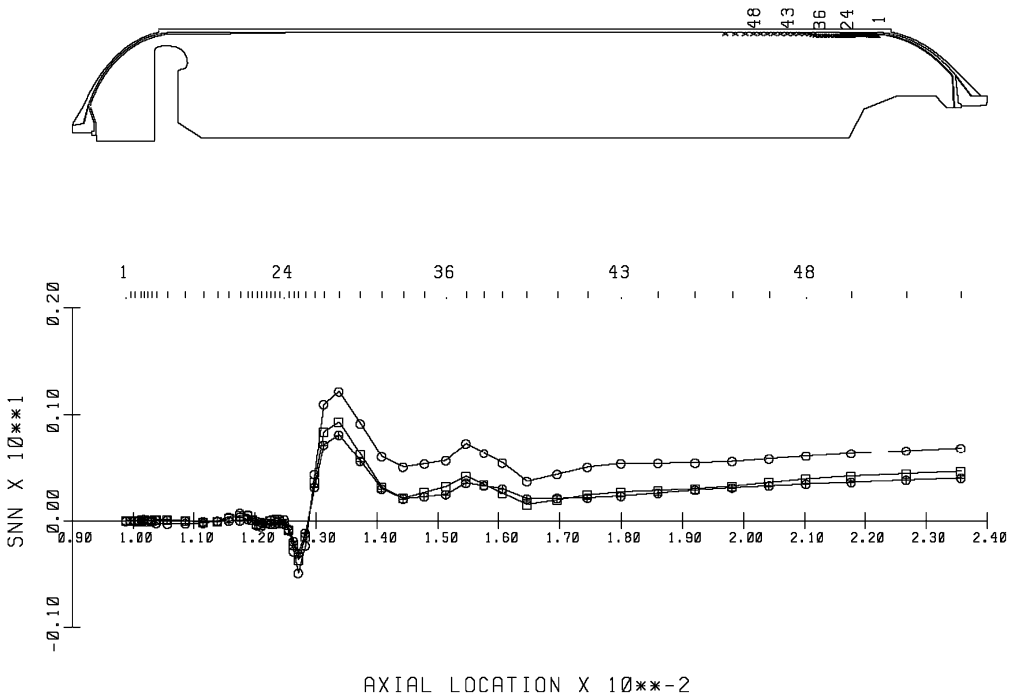

Fig. 8 Thermal-cycle bond stress for new propellant (first cycle ○, second cycle □, and third cycle ⊕).

02 kg/mm^2 was observed for the aged propellant at the end of the second step at the liner–insulation interface.

Ignition Pressurization

There are two loading steps for this analysis. The first step corresponds to the cooling down of the propellant, and the second step corresponds to the ignition pressurization. The first step was defined as one day cooling from 60°C to −20°C followed by four days of cooling to −32°C. The second step is ignition pressurization to 0.663 kg/mm^2 (943 psi) with a rise time of 0.363 s.

Two curves that show the distribution of hoop strain and of bond stress along relevant surfaces at the end of each step (cooldown to −30°C and pressurization) are shown in Figs. 11–13. The maximum hoop strain of 12.60% was observed for the new propellant at the end of the second step (pressurization) on the surface of the bore region. The maximum hoop strain of 13.60% was observed for the aged propellant at the end of the second step (pressurization) on the surface of the bore region. The maximum bond stress of 1.22E − 02 kg/mm^2 was observed for the new propellant at the end of the first step (cooldown) at the liner–insulation interface. The maximum bond stress of 2.68E − 02 kg/mm^2 was observed for the aged propellant at the end of the first step (cooldown) at the liner–insulation interface.

Summary of Finite Element Analysis Results

Maximum values of bond stress and hoop strain for the three loading conditions are reported in Table 1 for the new propellant and Table 2 for the aged propellant.

For the new propellant the maximum hoop strain of 12.60% was observed at the end of the second step of the Ignition Pressurization

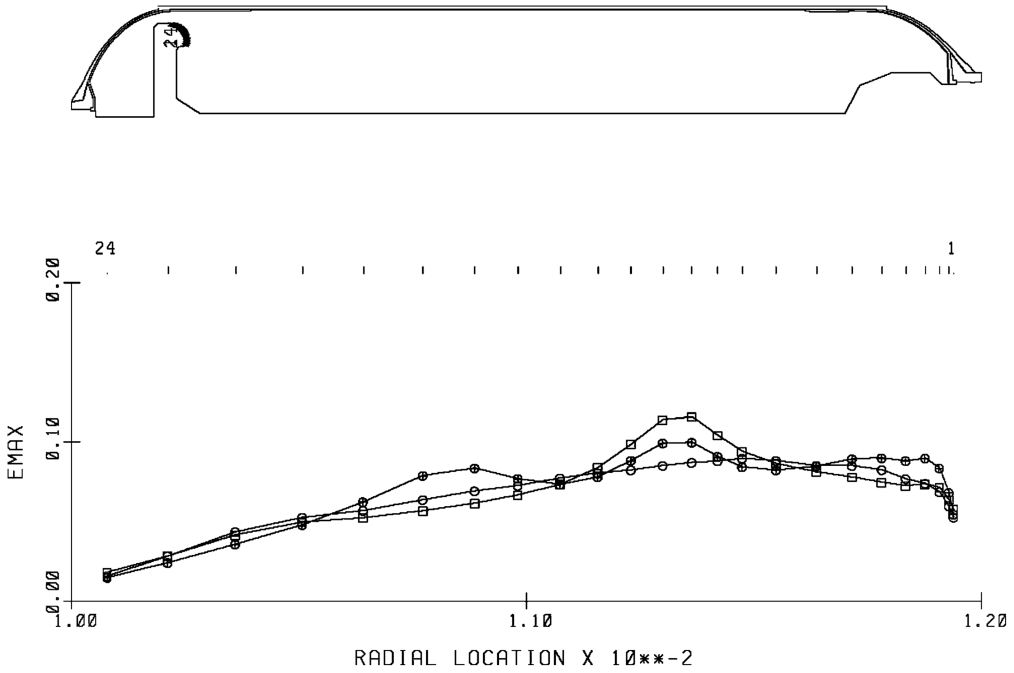

Fig. 9 Thermal-cycle hoop strains for aged propellant in the slot region (first cycle ○, second cycle □, and third cycle ⊕).

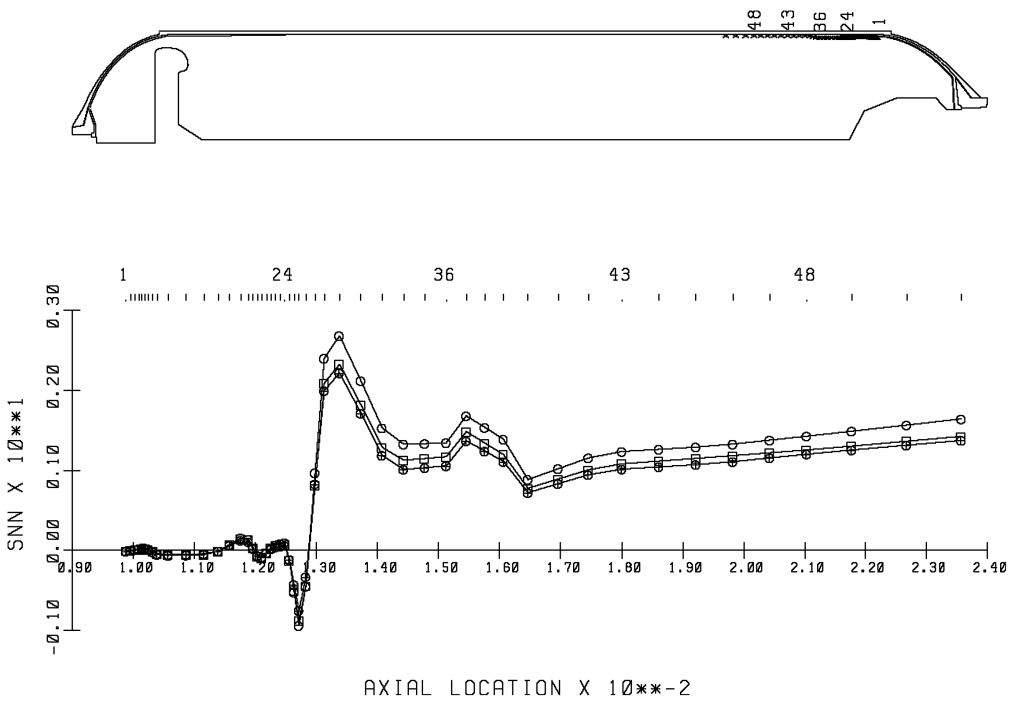

Fig. 10 Thermal-cycle bond stress for aged propellant (first cycle ○, second cycle □, and third cycle ⊕).

Analysis on the surface of the bore region. For the aged propellant, the maximum hoop strain of 13.60% was observed at the end of the second step of ignition pressurization analysis on the surface of the bore region.

For the new propellant the maximum bond stress of 1.22E − 02 kg/mm^2 was observed at the end of the first thermal cycle of thermal-cycling analysis and also at the end of the first step (cool down) of ignition pressurization analysis in both cases at the liner–insulation interface. For the aged propellant the maximum bond stress of 2.68E − 02 kg/mm^2 was observed at the end of the first thermal cycle of thermal-cycling analysis and also at the end of the first step (cool down) of ignition pressurization analysis, in both cases at the liner–insulation interface.

The finite element analysis results indicate only a slight change in the maximum hoop strain, while a large increase in the maximum bond stress as the propellant ages. The magnitude and location of these stresses and strains may be affected by the anisotropy of the case. The actual error induced in the results by the isotropic modeling of the case cannot be calculated without complete test data to determine the anisotropic material constants of the fiber-reinforced case. In the following, the predicted stress values are employed in the service-life estimation assuming that the error is not very significant, since the location of the maximum bond stress on the interface is far from the domes, where the case anisotropy is likely to have more influence on the stress predictions.

Service-Life Prediction

Service-life estimation is based on the ability to predict the future material properties, both response (stress–strain behavior) and

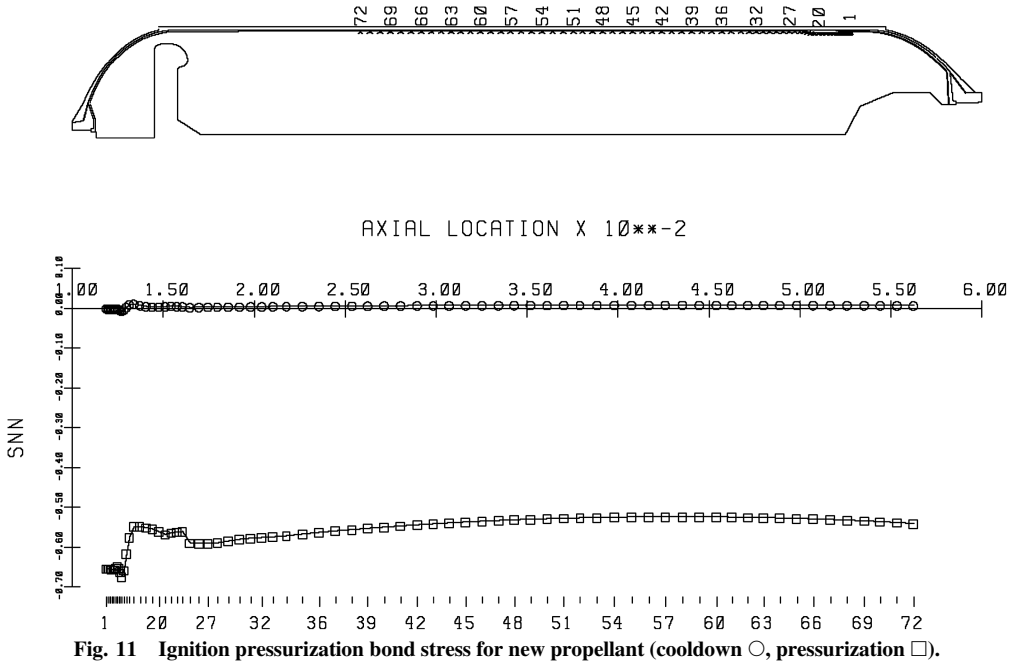

Fig. 11 Ignition pressurization bond stress for new propellant (cooldown ○, pressurization □).

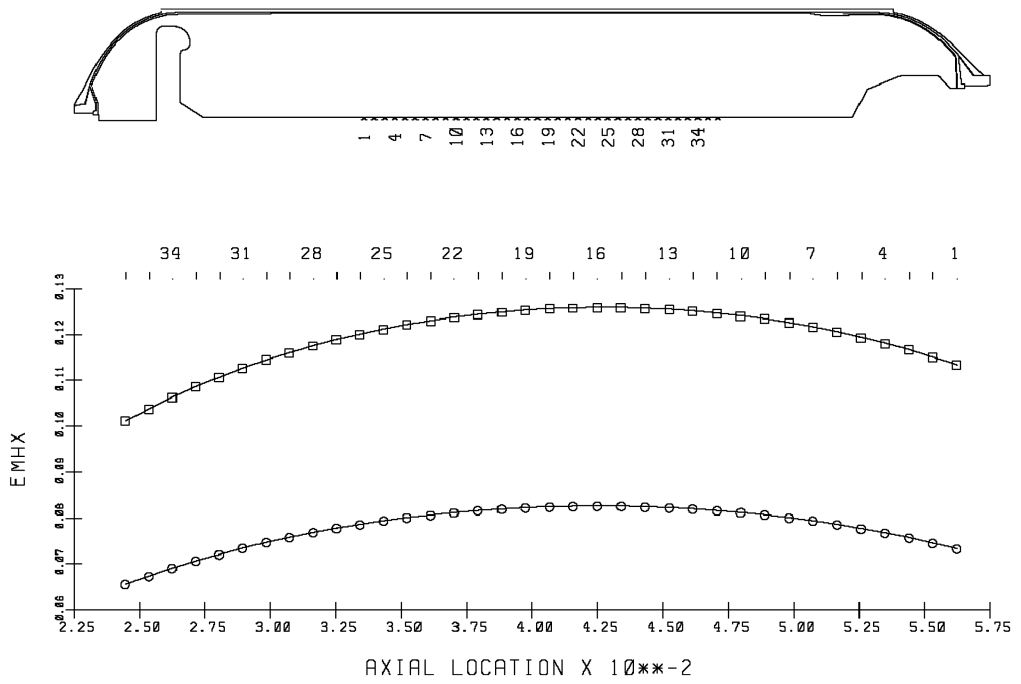

Fig. 12 Ignition pressurization hoop strain for new propellant in bore region (cooldown ○ and pressurization □).

capabilities (strength, ultimate strain, etc.) for the propellant and other elastomeric components. The description of the physical and chemical changes in propellant behavior is particularly important for a reasonable confidence in extrapolating current properties to future times. In this work the changes in propellant properties were predicted via an empirical approach, which is based on periodic testing of the propellant during the life of the motor. Since limited test data from aged samples were available, only one age was used for predicting stress–strain response, while data from four ages were used for predicting capabilities.

The prediction of the future material response consisted of the calibration of constitutive model for a six-year-old propellant, as described before. The finite element analysis of the motor with aged propellant was performed and the critical values of stress and strain were obtained.

Strain capability and bond-line strength, which are central to the determination of structural integrity, are rate and temperature dependent. The failure strain (strain at maximum stress) and maximum stress data were available at various strain rates and temperatures for the new propellant and at a single strain rate and temperature for the aged propellant samples. For the new propellant based on time–temperature equivalence and WLF shift function, master curves of strain capability were obtained. For the aged propellants Arrhenius rate equations were fitted to the available data and the resulting models were used to predict the master curves for ages 1, 2, 6, and 20 years. The results are shown in Fig. 14. The value of critical strain calculated in the finite element analysis of the cold-temperature motor ignition pressurization for the new and six-year-old propellants are also shown. It is clear from this figure that there is a large margin of safety for these two ages. Although the demand

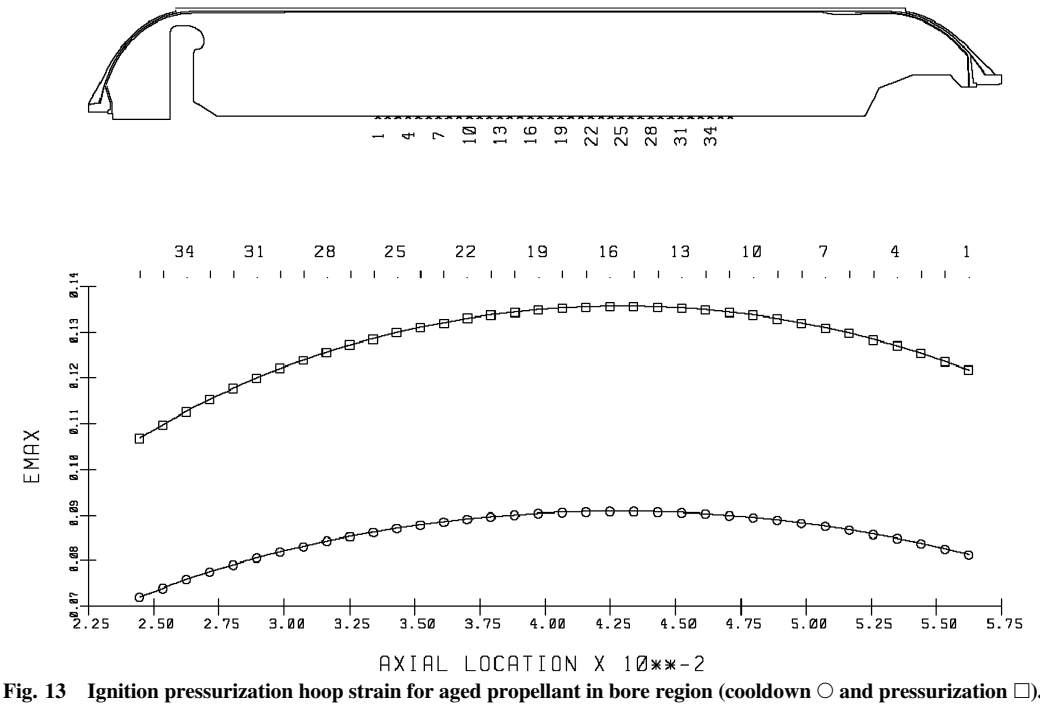

Fig. 13 Ignition pressurization hoop strain for aged propellant in bore region (cooldown ○ and pressurization □).

Table 1 Maximum-hoop-strain and bond-stress values and their locations for new propellant

Step	Location	Hoop strain	Bond stress, kg/mm^2
	Thermal cycling		
Third cycle	Slot	8.40E − 02	—
First cycle	Liner–insulation	—	1.22E − 02
	Thermal storage		
Coldest	Bore	6.55E − 02	—
Coldest	Liner–insulation	—	7.82E − 03
	Ignition pressurization		
Pressurization	Bore	1.26E − 01	—
Cooldown	Liner–insulation	—	1.22E − 02

Table 2 Maximum-hoop-strain and bond-stress values and their locations for aged propellant

Step	Location	Hoop strain	Bond stress, kg/mm^2
	Thermal cycling		
Second cycle	Slot	1.16E − 01	—
First cycle	Liner–insulation	—	2.68E − 02
	Thermal storage		
Coldest	Bore	7.01E − 02	—
Coldest	Liner–insulation	—	1.60E − 02
	Ignition pressurization		
Pressurization	Bore	1.36E − 01	—
Cooldown	Liner–insulation	—	2.68E − 02

cannot be determined for other ages without doing FEA for the older propellants, it is apparent that the value of critical strain does not change much with age.

A bond-stress master curve is obtained in a similar manner to that of the strain capability, as discussed above. The resulting strength capability curves for the new propellant, and in subsequent years, as calculated from the Arrhenius data, are shown in Fig. 15. Also shown are the demands for the new and the aged propellants. It is apparent that a large increase in bond stress is predicted by the finite element analysis. This is partially accommodated by the predicted increase in capability.

If the trends in bond-stress capability and demand continue, as suggested by the data given above, it is possible that at some future time the demand will exceed the capability, and bond failure would be predicted.

For an illustrative purpose, if it is assumed that the trends in bond strength and bond stress continue at the rate calculated, it can be estimated that after 25 years bond failure will occur during cold firing, as shown in Fig. 16. Confidence in this prediction is rather low, mainly due to incomplete data with respect to bond strength of aged propellant.

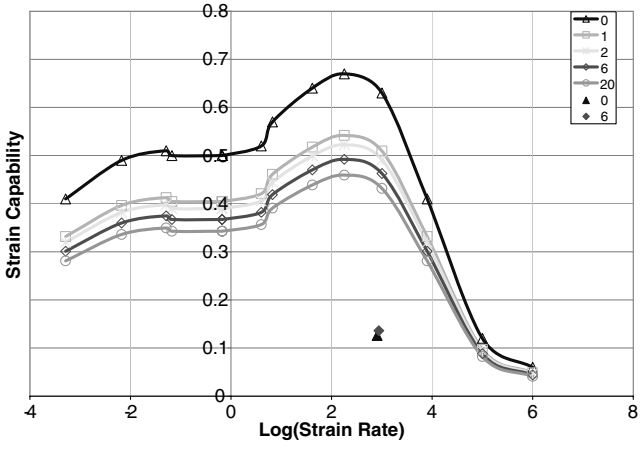

Fig. 14 Motor strain capability at various ages.

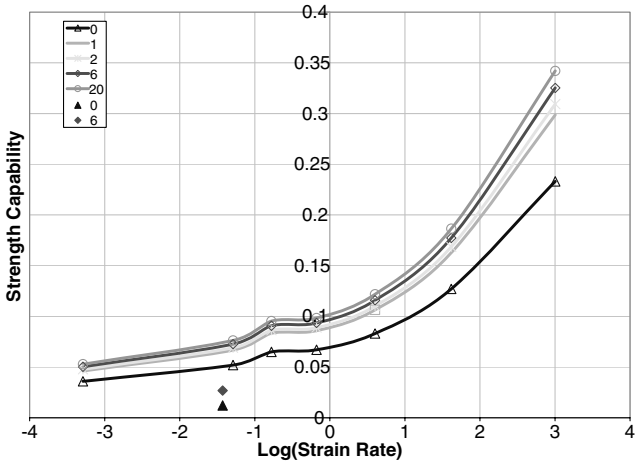

Fig. 15 Motor bond strength at various ages.

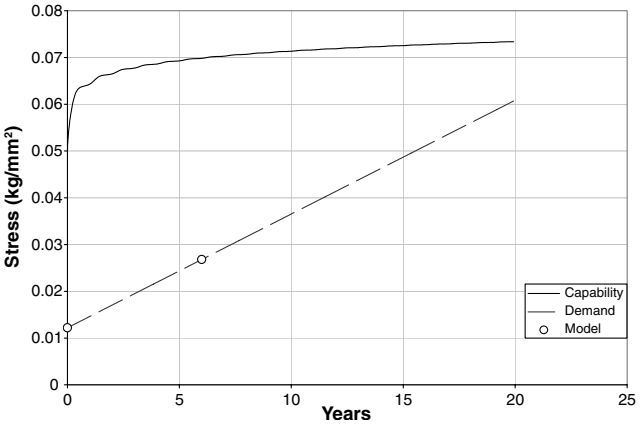

Fig. 16 Service-life prediction.

To make a more realistic quantitative estimate of the service life of the motor, the response and the capabilities data of the propellant and the propellant-liner–insulation bond system should be generated at regular intervals during the life of the motor. One possible method to accomplish this would be the mechanical testing of propellant samples scavenged from the rocket motors that have been subject to the thermal loading history of interest. At least three samples, preferably taken from different batches of propellant, should be used for each specimen tested. Periodic testing would allow establishing trends in response and capabilities hence increase the confidence in service-life prediction. Another method to accumulate data would be the usage of stress and temperature sensors embedded at critical locations of a rocket motor [18]. The sensors would be installed during the casting of the propellant grain; therefore, continuous measurements could be made during the life of the motor. The produced data would allow validation of the service-life prediction procedure as described in this study, as well as health monitoring of individual motors.

Conclusions

A procedure to predict the service life of a solid propellant rocket motor has been presented. The methodology is distinct from those previously proposed in the literature, since it is based on a comprehensive propellant model. Both the stress and dilatation responses are well represented and the model has been validated for multi-axial states that closely approximate actual motor conditions.

In this procedure, the effect of aging on the material response is included by calibrating the model for propellants at different ages. Because some of the necessary data (in particular, those from tensile tests run at different pressure levels) were not available, there is a lack

of certainty regarding fidelity of the propellant material model as calibrated.

Although the motor case material is fiber-reinforced plastic, only isotropic and homogeneous elastic properties were available. The effect of anisotropy on the stresses and strains in and near the domes should be evaluated to assess the validity of the stress analysis.

To determine strain capability and bond-line strength for future propellant ages, some history of change that occurs in these properties should be available. In this study limited capability data were available for the aged propellants; hence, Arrhenius models were used to calculate changes in capabilities. By collecting more extensive data for capabilities, more realistic extrapolation to future times would be possible.

The propellant model used in the study contains an internal state variable that measures the damage. Evaluation of this variable as predictor of material failure and definition of new internal variables to measure aging are considered as part of future study.

Acknowledgments

The author gratefully acknowledges the financial support of the Scientific and Technological Research Council of Turkey and the Turkish Scientific Research Projects Fund of Boğaziçi University.

References

[1] Simo, J. C., "On a Fully Three-Dimensional Finite-Strain Viscoelastic Damage Model: Formulation and Computational Aspects," *Computer Methods in Applied Mechanics and Engineering*, Vol. 60, 1987, pp. 153–173. doi:10.1016/0045-7825(87)90107-1

[2] Özüpek, Ş., and Becker, E. B., "Constitutive Modeling of High Elongation Solid Propellants," *Journal of Engineering Materials and Technology*, Vol. 114, 1992, pp. 111–115. doi:10.1115/1.2904130

[3] Özüpek, Ş., and Becker, E. B., "Constitutive Equations for Solid Propellants," *Journal of Engineering Materials and Technology*, Vol. 119, 1997, pp. 125–132. doi:10.1115/1.2805983

[4] Jung, G.-D., and Youn, S.-K., "A Nonlinear Viscoelastic Constitutive Model of Solid Propellant," *International Journal of Solids and Structures*, Vol. 36, 1999, pp. 3755–3777. doi:10.1016/S0020-7683(98)00175-9

[5] Matouš, K., and Geubelle, P. H., "Finite Element Formulation for Modeling Particle Debonding in Reinforced Elastomers Subjected to Finite Deformations," *Computer Methods in Applied Mechanics and Engineering*, Vol. 196, 2006, pp. 620–633. doi:10.1016/j.cma.2006.06.008

[6] Areias, P., and Matouš, K., "Finite Element Formulation for Modeling Nonlinear Viscoelastic Elastomers," *Computer Methods in Applied Mechanics and Engineering*, Vol. 197, 2008, pp. 4702–4717. doi:10.1016/j.cma.2008.06.015

[7] Xu, F., Aravas, N., and Sofronis, P., "Constitutive Modeling of Solid Propellant Materials with Evolving Microstructural Damage," *Journal of the Mechanics and Physics of Solids*, Vol. 56, 2008, pp. 2050–2073. doi:10.1016/j.jmps.2007.10.013

[8] Chyuan, S.-W., "A Study of Loading History Effect for Thermoviscoelastic Solid Propellant Grains," *Computers and Structures*, Vol. 77, 2000, pp. 735–745. doi:10.1016/S0045-7949(00)00009-2

[9] Chyuan, S.-W., "Nonlinear Thermoviscoelastic Analysis of Solid Propellant Grains Subjected to Temperature Loading," *Finite Elements in Analysis and Design*, Vol. 38, No. 7, 2002, pp. 613–630. doi:10.1016/S0168-874X(01)00095-6

[10] Christiansen, A. G., Layton, L. H., and Carpenter, R. L., "HTPB Propellant Aging," *Journal of Spacecraft and Rockets*, Vol. 18, 1981, pp. 211–214. doi:10.2514/3.57807

[11] Kivity, M., Hartman, G., and Achlama, A. M., "Aging of HTPB Propellant," 41st Propulsion Conference, Tucson, AZ, AIAA Paper 2005-3802, 2005.

[12] Huang, W., and Xing, Y., "Mechanical Property Prediction Method for HTPB Propellant Aging," 43rd Propulsion Conference, Cincinnati, OH, AIAA Paper 2007-5769, 2007.

[13] Ho, S. Y., "Viscoelastic Response of Solid Rocket Motor Components for Service Life Assessment," *Journal of Materials Science*, Vol. 32, 1997, pp. 5155–5161. doi:10.1023/A:1018677702953

[14] Collingwood, G. A., Clark, L. M., and Becker, E. B., "Solid Rocket Motor Service Life Prediction Using Nonlinear Viscoelastic Analysis and a Probabilistic Approach," *AGARD Conference Proceedings*, CP 586, AGARD, Neuilly-sur-Seine, France, 1997.

[15] *TEXPAC Computer Code User's Manual*, Mechanics Software, Inc., Austin, TX, 1989.

[16] Canga, M. E., Becker, E. B., and Özüpek Ş., "Constitutive Modeling of Viscoelastic Materials with Damage—Computational Aspects," *Computer Methods in Applied Mechanics and Engineering*, Vol. 190, 2001, pp. 2207–2226. doi:10.1016/S0045-7825(00)00231-0

[17] Williams, W. L., Landel, R. F., and Ferry, J. D., "The Temperature Dependence of Relaxation Mechanisms in Amorphous Polymers and Other Glass-Forming Liquids," *Journal of the American Chemical Society*, Vol. 77, 1955, pp. 3701–3707. doi:10.1021/ja01619a008

[18] Brouwer, G. R., Buswell, J. F., and Chelner, H., "The Use of Embedded Bond Stress Sensors to Determine Aging," AIAA Paper 2007-5788, July 2007.

P. Gage
Associate Editor